NUWC-NPT Technical Report 10,853
3 April 1995

6

The Phase Sensitivity of an Infinite Length Optical Fiber Subjected to a Forcing Function at a Definite Frequency and Wavenumber

Andrew J. Hull
Submarine Sonar Department

Naval Undersea Warfare Center Division
Newport, Rhode Island

PREFACE

The research described in this report was sponsored by the NUWC Division Newport Bid and Proposal (B&P) Program, which provides support for the preliminary, conceptual, and technical work necessary to generate complete and comprehensive proposals for direct-funded work. This effort was funded under Project No. 795P03, *A Model of the Refractive Index and Optical Phase Sensitivity of an Optical Fiber Subjected to a Dynamic External Force*, Principal Investigator A. J. Hull (Code 2141), NUWC Detachment New London.

The technical reviewer for this report was V. L. Go (Code 2141).

The author wishes to thank K. A. Holt for her help with the editing of the manuscript.

Reviewed and Approved: 3 April 1995

R J Martin

R. J. Martin
Acting Head, Submarine Sonar Department

REPORT DOCUMENTATION PAGE

Form Approved
OMB No. 0704-0188

1. AGENCY USE ONLY (Leave Blank)	2. REPORT DATE	3. REPORT TYPE AND DATES COVERED
	3 April 1995	Progress

4. TITLE AND SUBTITLE

The Phase Sensitivity of an Infinite Length Optical Fiber Subjected to a Forcing Function at a Definite Frequency and Wavenumber

5. FUNDING NUMBERS

6. AUTHOR(S)

Andrew J. Hull

7. PERFORMING ORGANIZATION NAME(S) AND ADDRESS(ES)

Naval Undersea Warfare Center
Detachment New London
New London, Connecticut 06320

8. PERFORMING ORGANIZATION REPORT NUMBER

TR 10,853

9. SPONSORING/MONITORING AGENCY NAME(S) AND ADDRESS(ES)

10. SPONSORING/MONITORING AGENCY REPORT NUMBER

11. SUPPLEMENTARY NOTES

12a. DISTRIBUTION/AVAILABILITY STATEMENT

Approved for public release; distribution is unlimited.

12b. DISTRIBUTION CODE

13. ABSTRACT (Maximum 200 words)

The model developed in this report provides an exact solution to the equations of motion for an infinite length, axisymmetric, isotropic, forced cylindrical rod. The resulting mechanical stresses are inserted into the governing equations of optical phase sensitivity and the change of refractive index for an optical fiber. This approach produces a closed-form model of light propagation in the fiber when the fiber is subjected to external forcing functions at a definite wavenumber and frequency. The closed-form solution is then compared to a finite element solution and to experimental data. It is shown that the optical phase sensitivity of an infinite length fiber is shear stress dominated. When the fiber is subjected to normal pressure, the frequency domain dynamics are extremely small. However, when the fiber is subjected to shear stress, a 20-dB drop in optical phase sensitivity results between 50 and 500 Hz. A low-wavenumber approximation of the model is included, and simulations show its accuracy to a wavenumber of at least 4000 rad/m at 50 Hz.

14. SUBJECT TERMS	15. NUMBER OF PAGES
Closed-Form Solution, Finite Element Solution, Forcing Function, Infinite Length Fiber, Optical Fiber, Phase Sensitivity, Refractive Index, Shear Stress	40
	16. PRICE CODE

17. SECURITY CLASSIFICATION OF REPORT	18. SECURITY CLASSIFICATION OF THIS PAGE	19. SECURITY CLASSIFICATION OF ABSTRACT	20. LIMITATION OF ABSTRACT
UNCLASSIFIED	UNCLASSIFIED	UNCLASSIFIED	SAR

TABLE OF CONTENTS

LIST OF ILLUSTRATIONS

LIST OF ILLUSTRATIONS (CONT'D)

LIST OF TABLES

THE PHASE SENSITIVITY OF AN INFINITE LENGTH OPTICAL FIBER SUBJECTED TO A FORCING FUNCTION AT A DEFINITE FREQUENCY AND WAVENUMBER

1. INTRODUCTION

The phase sensitivity of an optical fiber is proportional to the longitudinal and radial strain in the fiber (Lagakos and Bucaro, 1981). These strains are related to the displacement field of the fiber by partial derivatives of the displacements (Timoshenko and Goodier, 1934), and can be changed by varying the external load on the fiber. Thus, the propagation of light through the fiber can be modified by the application of a mechanical force to the fiber exterior. In general, the optical fiber can be modeled as an elastic solid. The displacement field of elastic rods has been studied by numerous researchers because of their use in many mechanical designs (Holden, 1951; Kaul and McCoy, 1964; Meeker and Meitzler, 1964; Graff, 1975). There has not, however, been a thorough investigation of the phase sensitivity of optical fibers subjected to a forced response at a definite frequency and wavenumber.

In this report, the effects of an infinite length, axisymmetric, isotropic rod subjected to an external load at a definite wavenumber and frequency are presented. The resulting mechanical stresses are used in fiber optic equations to determine the phase sensitivity and the change of refractive index of the fiber. The derivation begins with the partial differential equations of motion of an isotropic, elastic, slightly damped solid in cylindrical coordinates. The displacements are written as the sum of a dilatational component and an equivoluminal vector component. This approach allows the equations to be separated into a dilatational wave equation and three distortional (shear) wave equations. General solutions to these four wave equations are next determined. These general solutions are inserted at the diameter of the rod into the stress-strain relationships, which are equated to the externally applied loading function on the cylinder. Based on these relationships, a two-by-two system of linear equations is developed. The solution to the linear equations yields the displacements of the rod. The

strains are determined from these displacements and then inserted into equations that yield the optical phase sensitivity and the change of refractive index of the fiber.

2. SYSTEM MODEL AND CLOSED-FORM SOLUTION

The system model is a cylindrical, linear, isotropic medium whose motion is governed by the equation (Timoshenko and Goodier, 1934)

$$\mu\nabla^2\mathbf{u}+(\lambda+\mu)\nabla\nabla\bullet\mathbf{u}=\rho\frac{\partial^2\mathbf{u}}{\partial t^2}\ , \tag{1}$$

where ρ is the density; λ and μ are the Lamé constants; t is time; $\bullet$ denotes a vector dot product; $\mathbf{u}$ is the cylindrical coordinate displacement vector expressed as

$$\mathbf{u}=\begin{Bmatrix} u_r(r,\theta,z,t) \\ u_\theta(r,\theta,z,t) \\ u_z(r,\theta,z,t) \end{Bmatrix}\ , \tag{2}$$

with subscript r denoting the radial direction, θ denoting the angular direction, and z denoting the axial direction; ∇ is the gradient vector differential operator written in cylindrical coordinates as (Potter, 1978)

$$\nabla=\frac{\partial}{\partial r}i_r+\frac{1}{r}\frac{\partial}{\partial\theta}i_\theta+\frac{\partial}{\partial z}i_z\ , \tag{3}$$

with i_r denoting the unit vector in the r direction, i_θ denoting the unit vector in the θ direction, and i_z denoting the unit vector in the z direction; ∇^2 is the three-dimensional Laplace operator operating on vector $\mathbf{u}$ as

$$\nabla^2\mathbf{u}=\left(\nabla^2 u_r-\frac{u_r}{r^2}-\frac{2}{r^2}\frac{\partial u_\theta}{\partial\theta}\right)i_r+\left(\nabla^2 u_\theta-\frac{u_\theta}{r^2}+\frac{2}{r^2}\frac{\partial u_r}{\partial\theta}\right)i_\theta+\nabla^2 u_z i_z\ , \tag{4}$$

with ∇^2 operating on scalar u as

$$\nabla^2 u_{r,\theta,z}=\nabla\bullet\nabla u_{r,\theta,z}=\frac{1}{r}\frac{\partial}{\partial r}\left(r\frac{\partial u_{r,\theta,z}}{\partial r}\right)+\frac{1}{r^2}\frac{\partial^2 u_{r,\theta,z}}{\partial\theta^2}+\frac{\partial^2 u_{r,\theta,z}}{\partial z^2}\ ; \tag{5}$$

and the term $\nabla\bullet\mathbf{u}$ is called the divergence and is equal to

$$\nabla \bullet \mathbf{u} = \frac{\partial u_r}{\partial r} + \frac{1}{r}\frac{\partial u_\theta}{\partial \theta} + \frac{\partial u_z}{\partial z} + \frac{u_r}{r} \ . \tag{6}$$

The coordinate system of the rod is shown in figure 1.

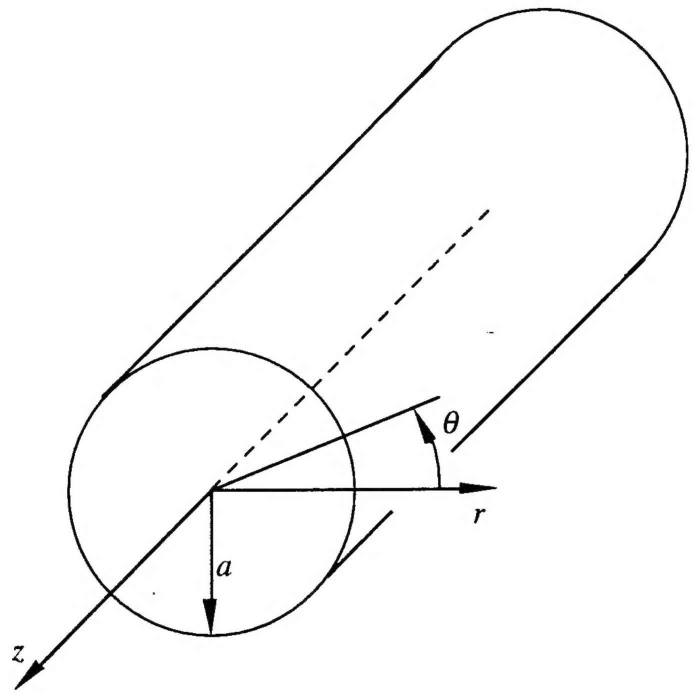

Figure 1. Cylindrical Rod

The displacement vector **u** is written as

$$\mathbf{u} = \nabla\phi + \nabla \times \mathbf{H} \ , \tag{7}$$

where ϕ is a dilatational scalar potential, $\times$ denotes a vector cross product, and **H** is an equivoluminal vector potential expressed as

$$\mathbf{H} = \begin{Bmatrix} H_r(r,\theta,z,t) \\ H_\theta(r,\theta,z,t) \\ H_z(r,\theta,z,t) \end{Bmatrix} \ . \tag{8}$$

Expanding equation (7) and breaking the displacement vector into its individual terms yields

$$u_r = \frac{\partial \phi}{\partial r} + \frac{1}{r}\frac{\partial H_z}{\partial \theta} - \frac{\partial H_\theta}{\partial z} \ , \tag{9}$$

$$u_\theta = \frac{1}{r}\frac{\partial \phi}{\partial \theta} + \frac{\partial H_r}{\partial z} - \frac{\partial H_z}{\partial r} , \tag{10}$$

and

$$u_z = \frac{\partial \phi}{\partial z} + \frac{H_\theta}{r} + \frac{\partial H_\theta}{\partial r} - \frac{1}{r}\frac{\partial H_r}{\partial \theta} . \tag{11}$$

Equation (7) is next inserted into equation (1), which results in

$$c_d^2 \nabla^2 \phi = \frac{\partial^2 \phi}{\partial t^2} \tag{12}$$

and

$$c_s^2 \nabla^2 \mathbf{H} = \frac{\partial^2 \mathbf{H}}{\partial t^2} . \tag{13}$$

The constants c_d and c_s are the complex dilatational and shear wave speeds, respectively, and are determined by

$$c_d = \sqrt{\frac{\lambda + 2\mu}{\rho}} \tag{14}$$

and

$$c_s = \sqrt{\frac{\mu}{\rho}} . \tag{15}$$

The relationship of the Lamé constants to the compressional and shear moduli is shown as

$$\lambda = \frac{E\upsilon}{(1+\upsilon)(1-2\upsilon)} \tag{16}$$

and

$$\mu = G = \frac{E}{2(1+\upsilon)} , \tag{17}$$

where E is the complex compressional modulus (N/m^2), G is the complex shear modulus (N/m^2), and υ is the Poisson's ratio of the material (dimensionless).

The conditions of infinite length, axisymmetric response (n = 0), and steady-state response are now imposed, allowing the scalar and vector potential to be written as

$$\phi = g(r)\cos(n\theta)e^{ikz}e^{i\omega t} = g(r)e^{ikz}e^{i\omega t} \ , \tag{18}$$

$$H_r = h_r(r)\sin(n\theta)e^{ikz}e^{i\omega t} \equiv 0 \ , \tag{19}$$

$$H_\theta = h_\theta(r)\cos(n\theta)e^{ikz}e^{i\omega t} = h_\theta(r)e^{ikz}e^{i\omega t} \ , \tag{20}$$

and

$$H_z = h_z(r)\sin(n\theta)e^{ikz}e^{i\omega t} \equiv 0 \ , \tag{21}$$

where k is the wavenumber of excitation, ω is the frequency of excitation, and i is the square root of -1. Note that for axisymmetric response, the equations of motion are dependent only on the scalar potential ϕ and angular contribution H_θ of the vector potential. Additionally, because $H_r = 0$, $H_z = 0$, and H_θ and ϕ are not functions of θ, equation (10) becomes

$$u_\theta = \frac{\partial(\,)}{\partial\theta} = 0 \ , \tag{22}$$

where ( ) denotes any function. Inserting equations (18)-(21) into equations (12) and (13) yields the following four wave equations:

$$\frac{d^2g(r)}{dr^2} + \frac{1}{r}\frac{dg(r)}{dr} + \left(\frac{\omega^2}{c_d^2} - k^2\right)g(r) = 0 \ , \tag{23}$$

$$\frac{d^2h_r(r)}{dr^2} + \frac{1}{r}\frac{dh_r(r)}{dr} + \left(\frac{\omega^2}{c_s^2} - k^2 - \frac{1}{r^2}\right)h_r(r) = 0 \ , \tag{24}$$

$$\frac{d^2h_\theta(r)}{dr^2} + \frac{1}{r}\frac{dh_\theta(r)}{dr} + \left(\frac{\omega^2}{c_s^2} - k^2 - \frac{1}{r^2}\right)h_\theta(r) = 0 \ , \tag{25}$$

and

$$\frac{d^2h_z(r)}{dr^2} + \frac{1}{r}\frac{dh_z(r)}{dr} + \left(\frac{\omega^2}{c_s^2} - k^2\right)h_z(r) = 0 \ . \tag{26}$$

The solution to equations (23) and (25) is now found with a Bessel function. No solution is found to equations (24) and (26) because they do not contribute to the axisymmetric response. The solution to equation (23) is

$$g(r) = C_1 J_0(\alpha r) \ , \tag{27}$$

where J_0 is a complex, zero-order, first-kind standard Bessel function; C_1 is a complex constant (determined below); and

$$\alpha = \sqrt{\frac{\omega^2}{c_d^2} - k^2} \ . \tag{28}$$

The solution to equation (23) is

$$h_\theta(r) = C_2 J_1(\beta r) \ , \tag{29}$$

where J_1 is a complex, first-order, first-kind standard Bessel function; C_2 is a complex constant (determined below); and

$$\beta = \sqrt{\frac{\omega^2}{c_s^2} - k^2} \ . \tag{30}$$

The numerical evaluation of the complex-valued Bessel functions is described in the appendix.

The displacements and external forces are now equated by use of the stress-strain constitutive equations on the forced surfaces of the rod. The normal stress, strain, and radial forces acting on the cylinder are related by

$$\sigma_{rr}(a,\theta,z,t) = (\lambda + 2\mu)\varepsilon_{rr}(a,\theta,z,t) + \lambda\varepsilon_{\theta\theta}(a,\theta,z,t) + \lambda\varepsilon_{zz}(a,\theta,z,t) = p(a,\theta,z,t) \ , \tag{31}$$

where $\sigma_{rr}(a,\theta,z,t)$ is the normal radial stress, $\varepsilon_{rr}(a,\theta,z,t)$ is the normal radial strain, $\varepsilon_{\theta\theta}(a,\theta,z,t)$ is the normal circumferential strain, $\varepsilon_{zz}(a,\theta,z,t)$ is the normal longitudinal strain, $p(a,\theta,z,t)$ is the external pressure on the cylinder in the radial direction, and a denotes the outer radius. The shear stress, strain, and longitudinal forces are related using

$$\sigma_{rz}(a,\theta,z,t) = 2\mu\varepsilon_{rz}(a,\theta,z,t) = f(a,\theta,z,t) \ , \tag{32}$$

where $\sigma_{rz}(a,\theta,z,t)$ is the shear stress, $\varepsilon_{rz}(a,\theta,z,t)$ is the shear strain, and $f(a,\theta,z,t)$ is the external shear stress on the rod in the longitudinal direction.

The strains are related to the displacements in an axisymmetric solid by (Timoshenko and Goodier, 1934)

$$\varepsilon_{rr} = \frac{\partial u_r}{\partial r} \ , \tag{33}$$

$$\varepsilon_{\theta\theta} = \frac{u_r}{r} \ , \tag{34}$$

$$\varepsilon_{zz} = \frac{\partial u_z}{\partial z} \ , \tag{35}$$

and

$$\varepsilon_{rz} = \frac{1}{2}\left(\frac{\partial u_z}{\partial r} + \frac{\partial u_r}{\partial z}\right) . \tag{36}$$

The relationship between the displacements (and the derivatives of the displacements) and the potential functions g and h_θ is found by combining equations (9), (11), (18), and (20) to produce

$$u_r = \left(\frac{dg(r)}{dr} - ikh_\theta(r)\right)e^{ikz}e^{i\omega t} \ , \tag{37}$$

$$u_z = \left(ikg(r) + \frac{h_\theta(r)}{r} + \frac{dh_\theta(r)}{dr}\right)e^{ikz}e^{i\omega t} \ , \tag{38}$$

$$\frac{\partial u_r}{\partial r} = \left(\frac{d^2 g(r)}{dr^2} - ik\frac{dh_\theta(r)}{dr}\right)e^{ikz}e^{i\omega t} \ , \tag{39}$$

$$\frac{\partial u_z}{\partial z} = \left(-k^2 g(r) + \frac{ikh_\theta(r)}{r} + ik\frac{dh_\theta(r)}{dr}\right)e^{ikz}e^{i\omega t} \ , \tag{40}$$

$$\frac{\partial u_z}{\partial r} = \left(ik\frac{dg(r)}{dr} + \frac{1}{r}\frac{dh_\theta(r)}{dr} - \frac{h_\theta(r)}{r^2} + \frac{d^2 h_\theta(r)}{dr^2}\right)e^{ikz}e^{i\omega t} \ , \tag{41}$$

and

$$\frac{\partial u_r}{\partial z} = \left(ik\frac{dg(r)}{dr} + k^2 h_\theta(r)\right)e^{ikz}e^{i\omega t} \ . \tag{42}$$

Combining equations (31), (33), (34), (35), (37), (39), and (40) yields the normal stress in terms of the potential functions g and h_θ at $r = a$ as

$$(\lambda + 2\mu)\frac{d^2 g(a)}{dr^2} + \frac{\lambda}{a}\frac{dg(a)}{dr} - \lambda k^2 g(a) - 2\mu ik\frac{d^2 h_\theta(a)}{dr^2} = P \ , \tag{43}$$

where P is the magnitude of the normal force acting on the exterior of the cylinder. Combining equations (32), (36), (41), and (42) yields the shear stress in terms of the potential functions g and h_θ at $r = a$. The result is

$$2\mu ik\frac{dg(a)}{dr} + \left(\mu k^2 - \frac{\mu}{a^2}\right)h_\theta(a) + \frac{\mu}{a}\frac{dh_\theta(a)}{dr} + \mu\frac{d^2h_\theta(a)}{dr^2} = F \ , \tag{44}$$

where F is the magnitude of the externally applied shear stress acting on the exterior of the rod. Implicit in equations (43) and (44) is the assumption that the external loads on the cylinder are occurring at a definite frequency and wavenumber.

Inserting equations (27) and (29) into equations (43) and (44), applying the recurrence relationships of the first-kind standard Bessel function, and then rewriting as a two-by-two system of linear equations results in

$$\begin{bmatrix} a_{11} & a_{12} \\ a_{21} & a_{22} \end{bmatrix} \begin{Bmatrix} C_1 \\ C_2 \end{Bmatrix} = \begin{Bmatrix} P \\ F \end{Bmatrix} , \tag{45}$$

where the matrix coefficients a_{nm} are given as

$$a_{11} = \left[(-\lambda - 2\mu)\alpha^2 - \lambda k^2\right]J_0(\alpha a) + \left(\frac{2\mu\alpha}{a}\right)J_1(\alpha a) \ , \tag{46}$$

$$a_{12} = (-2\mu ik\beta)J_0(\beta a) + \left(\frac{2\mu ik}{a}\right)J_1(\beta a) \ , \tag{47}$$

$$a_{21} = (-2\mu ik\alpha)J_1(\alpha a) \ , \tag{48}$$

and

$$a_{22} = [\mu(k^2 - \beta^2)]J_1(\beta a) \ . \tag{49}$$

The radial displacement of the rod, now found using equations (27), (29), and (37) and the constants C_1 and C_2 from equation (45), is given as

$$u_r(r,z,t) = \left[-C_1\alpha J_1(\alpha r) - C_2 ikJ_1(\beta r)\right]e^{ikz}e^{i\omega t} \ , \tag{50}$$

which can also be written as

$$u_r(r,z,t) = U_r(r)e^{ikz}e^{i\omega t} \ . \tag{51}$$

The longitudinal displacement of the cylinder is found using equations (27), (29), and (38), and is written as

$$u_z(r,z,t) = \left[C_1 ik J_0(\alpha r) + C_2 \beta J_0(\beta r)\right] e^{ikz} e^{i\omega t} \tag{52}$$

or

$$u_z(r,z,t) = U_z(r) e^{ikz} e^{i\omega t} \ . \tag{53}$$

The strains are evaluated at $r = 0$ because light propagation is confined primarily to the middle of the fiber. The radial strain of the rod from equation (33) is

$$\varepsilon_{rr}(0,z,t) = \left[-C_1\left(\frac{\alpha^2}{2}\right) - C_2\left(\frac{ik\beta}{2}\right)\right] e^{ikz} e^{i\omega t} \ . \tag{54}$$

The longitudinal strain, found from equation (35), is

$$\varepsilon_{zz}(0,z,t) = \left[-C_1 k^2 + C_2 (ik\beta)\right] e^{ikz} e^{i\omega t} \ . \tag{55}$$

The strains are related to the optical phase sensitivity by the equation

$$\frac{\Delta\phi}{\phi} = \varepsilon_{zz} - \frac{n_0^2}{2}\left[\varepsilon_{rr}(P_{11} + P_{12}) + \varepsilon_{zz} P_{12}\right] , \tag{56}$$

where n_0 is the refractive index of the fiber, and P_{11} and P_{12} are the Pockels' coefficients. Inserting the values of $n_0 = 1.46$, $P_{11} = 0.126$, and $P_{12} = 0.270$ changes equation (56) to

$$\frac{\Delta\phi}{\phi} = 0.712\varepsilon_{zz} - 0.422\varepsilon_{rr} \ . \tag{57}$$

The strains are related to the change of refractive index by the equation

$$dn = \frac{-n_0^3}{2}\left[2\varepsilon_{rr}(P_1 - P_4) + \varepsilon_{zz}(P_1 - 2P_4)\right] , \tag{58}$$

where $P_1 = P_{11} = 0.126$ and $P_4 = (P_{11}\text{-}P_{12}) / 2 = \text{-}0.0718$. Inserting these values changes equation (58) to

$$dn = -0.616\,\varepsilon_{rr} - 0.420\,\varepsilon_{zz} \ . \tag{59}$$

The above equations show that given the physical properties of the fiber and an external forcing function at a definite wavenumber and frequency, the optical phase sensitivity and the change of refractive index can be calculated in a closed-form solution.

3. FINITE ELEMENT SOLUTION

The closed-form solutions (equations (57) and (59)) are compared to results obtained with finite element analysis for the specific case of an external normal force applied at zero wavenumber. Finite element analysis is a discretized modeling technique that breaks down the structure into a number of subdomains (elements) (Cook, 1974; Zienkiewicz, 1983). Constitutive equations are applied to each of these elements to develop equations of motion. The individual equations of motion are then assembled to form a global equation:

$$\mathbf{M}\frac{d^2\mathbf{g}(t)}{dt^2}+\mathbf{C}\frac{d\mathbf{g}(t)}{dt}+\mathbf{K}\mathbf{g}(t)=\mathbf{f}(x,t)\ , \tag{60}$$

where **M** is the system mass matrix, **C** is the system damping matrix, **K** is the system stiffness matrix, $\mathbf{g}(t)$ is the generalized displacement vector, and $\mathbf{f}(x,t)$ is the external forcing function vector. The finite element results displayed here were obtained using ANSYS, which is a general purpose finite element computer program. Finite element analysis has the advantage of handling material and property discontinuities that are not easily resolved with other numerical techniques. It is routinely used for comparisons with other experiments and theories to verify results. It is important to note that, although the finite element analysis is an approximate numerical technique, it is extremely different from the analytical solution presented in section 2.

The finite element grid of the fiber is shown in figure 2. Because the elements in this analysis are axisymmetric, the torsional motion of the rod is zero. The problem was discretized with 10 elements in the radial direction and was loaded with a normal forcing function (harmonic in time) on the exterior of the cylinder. The forcing function had no spatial variation and therefore was equivalent to zero wavenumber excitation. The outputs of the finite element

program are longitudinal and radial stress; these values were inserted into equations (57) and (59) for comparison of the finite element method to the closed-form solution.

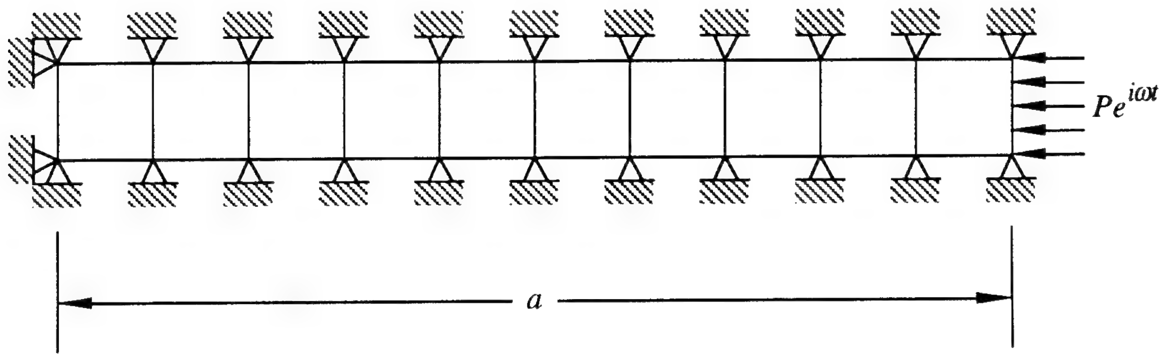

Figure 2. Finite Element Grid

4. ANALYSIS

An analysis of an optical fiber with the above mathematical methods was performed. The following mechanical parameters were used: $a = 62.5 \times 10^{-6}$ m, $E = 7.2 \times 10^{10}$ (1 + 0.01i) N/m^2, $\upsilon = 0.17$ (dimensionless), and $\rho = 2200$ kg/m^3. The test case of $f = 50$ Hz, $k = 0$, $F = 0$, and $P = 1$ N/m^2 is used for model verification. These results are listed in table 1. The experimental results in the table are from a previous study (Davis et al., 1982). Note that all three methods show results within 0.16 dB of each other.

Table 1. Comparison of Results at Zero Wavenumber

Method	$\lvert \Delta\phi / \phi P \rvert$ (m^2/N)	$\lvert \Delta\phi / \phi P \rvert$ (dB ref m^2/N)
Closed-Form Model	4.54×10^{-12}	-226.86
Finite Element Model	4.58×10^{-12}	-226.78
Experiment	4.50×10^{-12}	-226.94

The wavenumber analysis of the model was conducted at two frequencies: 50 and 500 Hz. This analysis was accomplished by first setting $F = 0$ and $P = 1$ N/m^2 to determine the optical response of the fiber to a normal pressure excitation of unity and by next setting $F = 1$ N/m^2 and $P = 0$ to calculate the optical response of the fiber to a shear force excitation of unity. In figures 3-18, the short dashed line represents the dilatational wavenumber ($k_d = \omega / c_d$) and the long dashed line represents the shear wavenumber ($k_s = \omega / c_s$). The exponential functions in time and space that are associated with the closed-form solution are suppressed.

Figure 3 is a plot of the transfer function of longitudinal strain divided by normal pressure versus wavenumber for $f = 50$ Hz. Figure 4 is a plot of the transfer function of radial strain divided by normal pressure versus wavenumber for $f = 50$ Hz. Figure 5 is a plot of the transfer function of optical phase sensitivity divided by normal pressure versus wavenumber for $f = 50$ Hz. Figure 6 is a plot of the transfer function of change of refractive index divided by normal pressure versus wavenumber for $f = 50$ Hz. Figure 7 is a plot of the transfer function of longitudinal strain divided by shear stress versus wavenumber for $f = 50$ Hz. Figure 8 is a plot of the transfer function of radial strain divided by shear stress versus wavenumber for $f = 50$ Hz. Figure 9 is a plot of the transfer function of optical phase sensitivity divided by shear stress versus wavenumber for $f = 50$ Hz. Figure 10 is a plot of the transfer function of change of refractive index divided by shear stress versus wavenumber for $f = 50$ Hz.

Figure 11 is a plot of the transfer function of longitudinal strain divided by normal pressure versus wavenumber for $f = 500$ Hz. Figure 12 is a plot of the transfer function of radial strain divided by normal pressure versus wavenumber for $f = 500$ Hz. Figure 13 is a plot of the transfer function of optical phase sensitivity divided by normal pressure versus wavenumber for $f = 500$ Hz. Figure 14 is a plot of the transfer function of change of refractive index divided by normal pressure versus wavenumber for $f = 500$ Hz. Figure 15 is a plot of the transfer function of longitudinal strain divided by shear stress versus wavenumber for $f = 500$ Hz. Figure 16 is a plot of the transfer function of radial strain divided by shear stress

versus wavenumber for $f = 500$ Hz. Figure 17 is a plot of the transfer function of optical phase sensitivity divided by shear stress versus wavenumber for $f = 500$ Hz. Figure 18 is a plot of the transfer function of change of refractive index divided by shear stress versus wavenumber for $f = 500$ Hz.

Comparing the fiber response to normal excitation (figures 3-6 and figures 11-14) and the fiber response to shear excitation (figures 7-10 and figures 15-18) shows that the fiber is 120 dB more sensitive to shear excitation than to normal excitation at 50 Hz and is 100 dB more sensitive to shear excitation than to normal excitation at 500 Hz. The response to normal excitation has relatively little change from 50 to 500 Hz. This implies that the time or frequency dynamics associated with a normal load on the fiber (and a corresponding response at $r = 0$) are extremely small. This was confirmed by analyzing the finite element model with static excitation, which produced results identical to a dynamic excitation at frequency $f = 50$ Hz. The fiber response to shear excitation is a decreased response of 20 dB from 50 to 500 Hz. In all the figures, the maximum response is occurring very close to the dilatational wavenumber. Additionally, the response around the shear wavenumber is flat, indicating that there is no shear wave propagation in the structure.

The above closed-form solution (equations (1)-(59)) can be simplified for low-wavenumber regions with linear approximations to the Bessel functions. Use of the small argument assumptions allows the Bessel functions to be written as

$$J_0(z) \approx 1 \tag{61}$$

and

$$J_1(z) \approx \frac{z}{2} \; . \tag{62}$$

Using equations (61) and (62), the matrix coefficients a_{nm} in equation (45) can be rewritten as

$$a_{11} = -\lambda\left(\frac{\omega}{c_d}\right)^2 - \mu\alpha^2 \; , \tag{63}$$

$$a_{12} = -\mu ik\beta \; , \tag{64}$$

$$a_{21} = -\mu ik\alpha^2 a \ , \tag{65}$$

and

$$a_{22} = \frac{\mu k^2 \beta a}{2} - \frac{\mu \beta^3 a}{2} \ . \tag{66}$$

The strains are evaluated using equations (54) and (55), with the constants C_1 and C_2 determined by equations (63)-(66). This expression of the closed-form solution is slightly different than that derived earlier because it contains the low-wavenumber assumption. The low-wavenumber solution was compared to the exact closed-form solution. The results are nearly identical up to a wavenumber of 1000 rad/m and vary only by 0.2 dB at a wavenumber of 4000 rad/m (for calculations at 50 Hz). For most applications, the low-wavenumber assumption is adequate to describe the response of the fiber.

5. CONCLUSIONS

The optical phase sensitivity of an infinite length fiber is shear stress dominated. When the fiber is subjected to a normal pressure, the frequency domain dynamics are extremely small. When the fiber is subjected to a shear stress, there is a 20-dB drop in the optical phase sensitivity between 50 and 500 Hz. The low-wavenumber assumption is accurate to model the response of the fiber up to a wavenumber of at least 4000 rad/m.

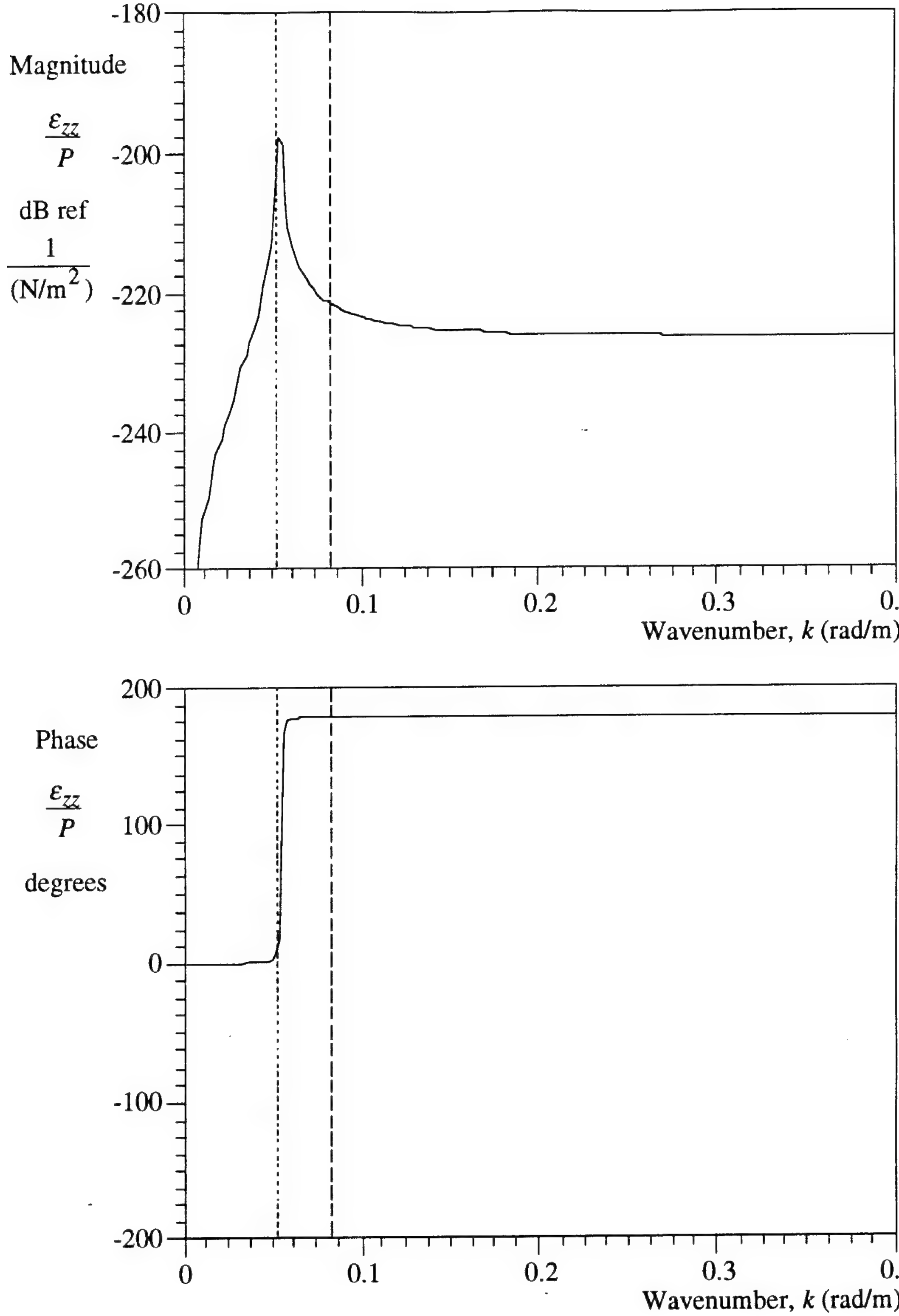

Figure 3. Transfer Function of Longitudinal Strain Divided by Normal Pressure Versus Wavenumber for $f = 50$ Hz

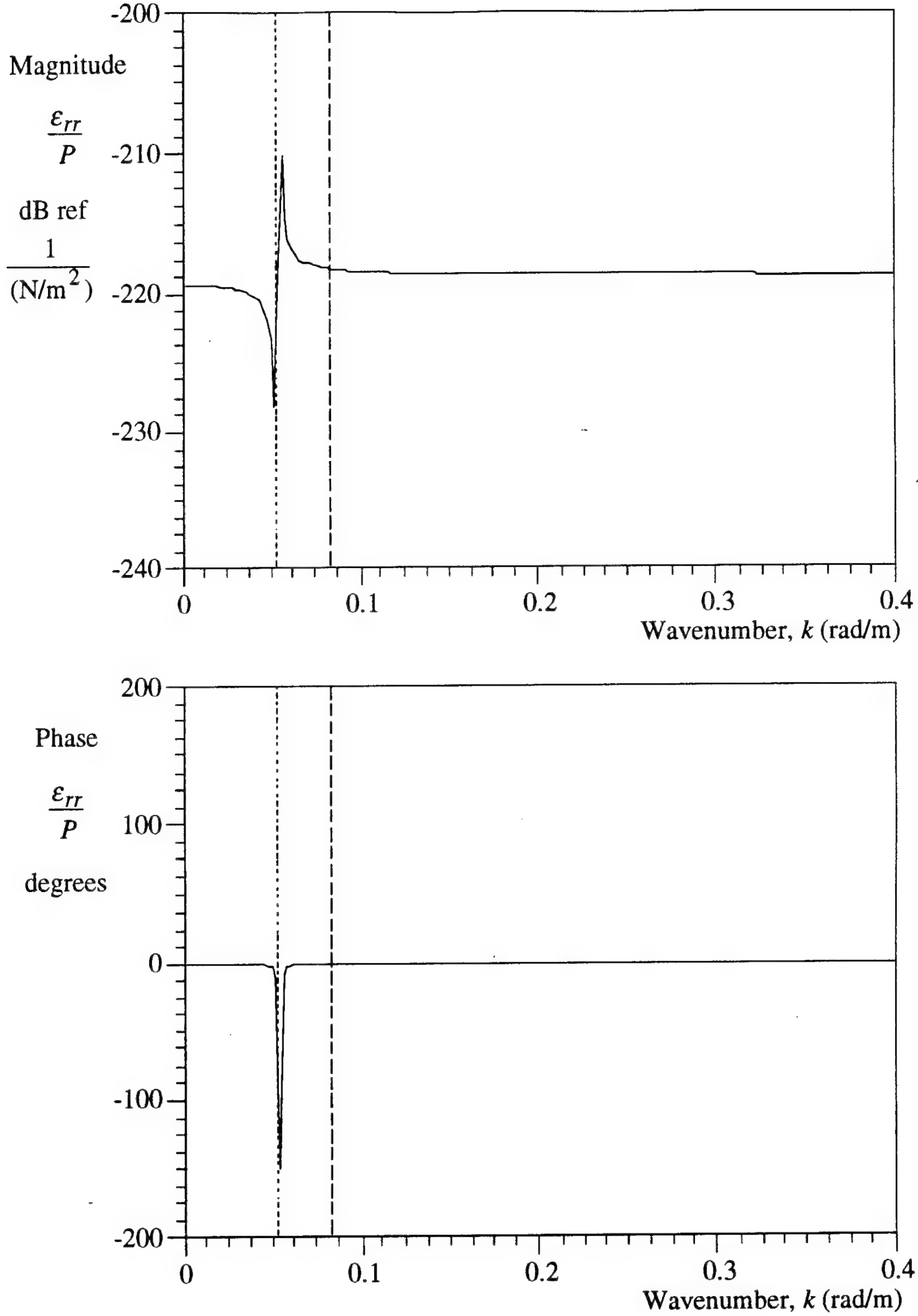

Figure 4. Transfer Function of Radial Strain Divided by Normal Pressure Versus Wavenumber for $f = 50$ Hz

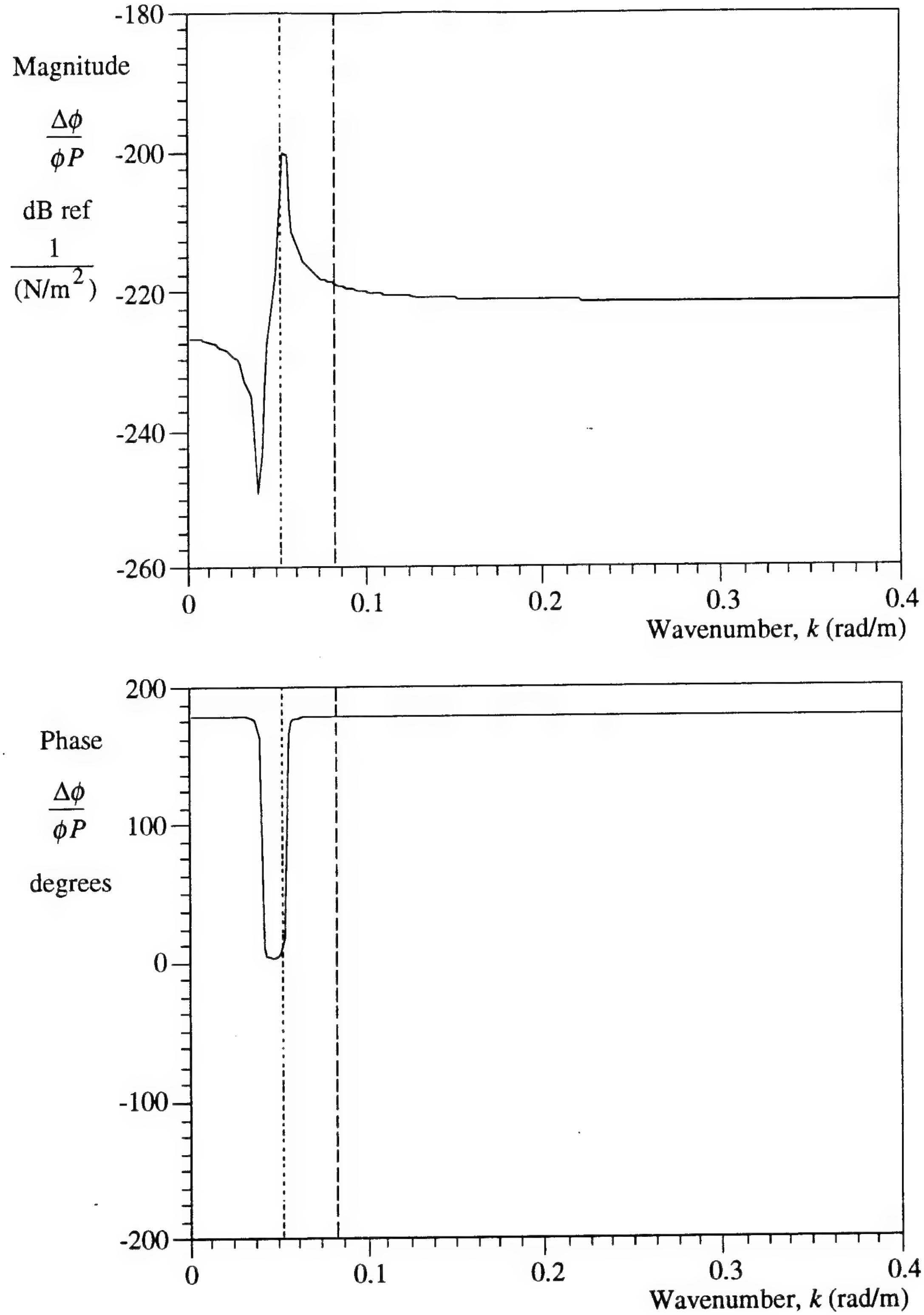

Figure 5. Transfer Function of Optical Phase Sensitivity Divided by Normal Pressure Versus Wavenumber for $f = 50$ Hz

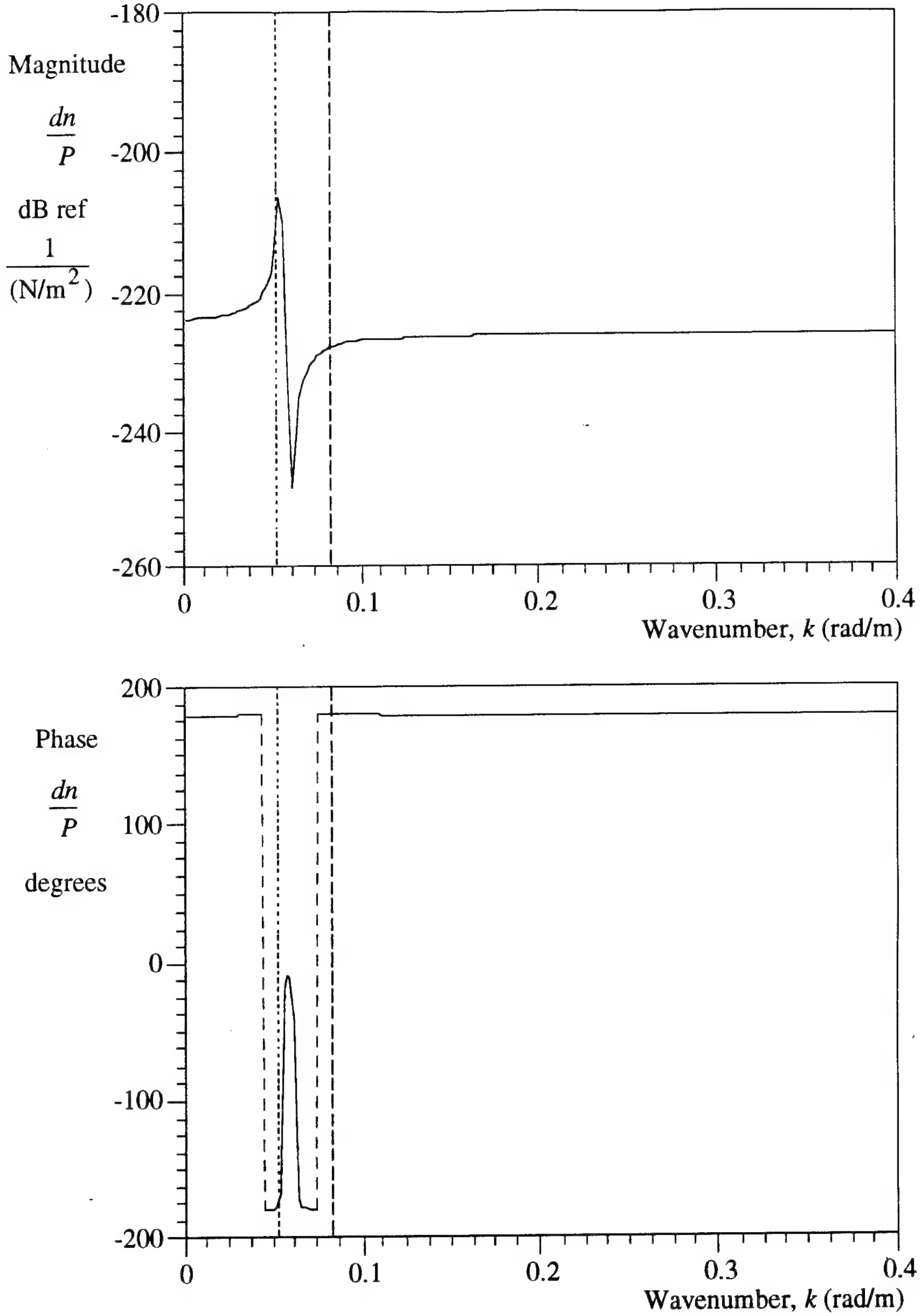

Figure 6. Transfer Function of Change of Refractive Index Divided by Normal Pressure Versus Wavenumber for $f = 50$ Hz

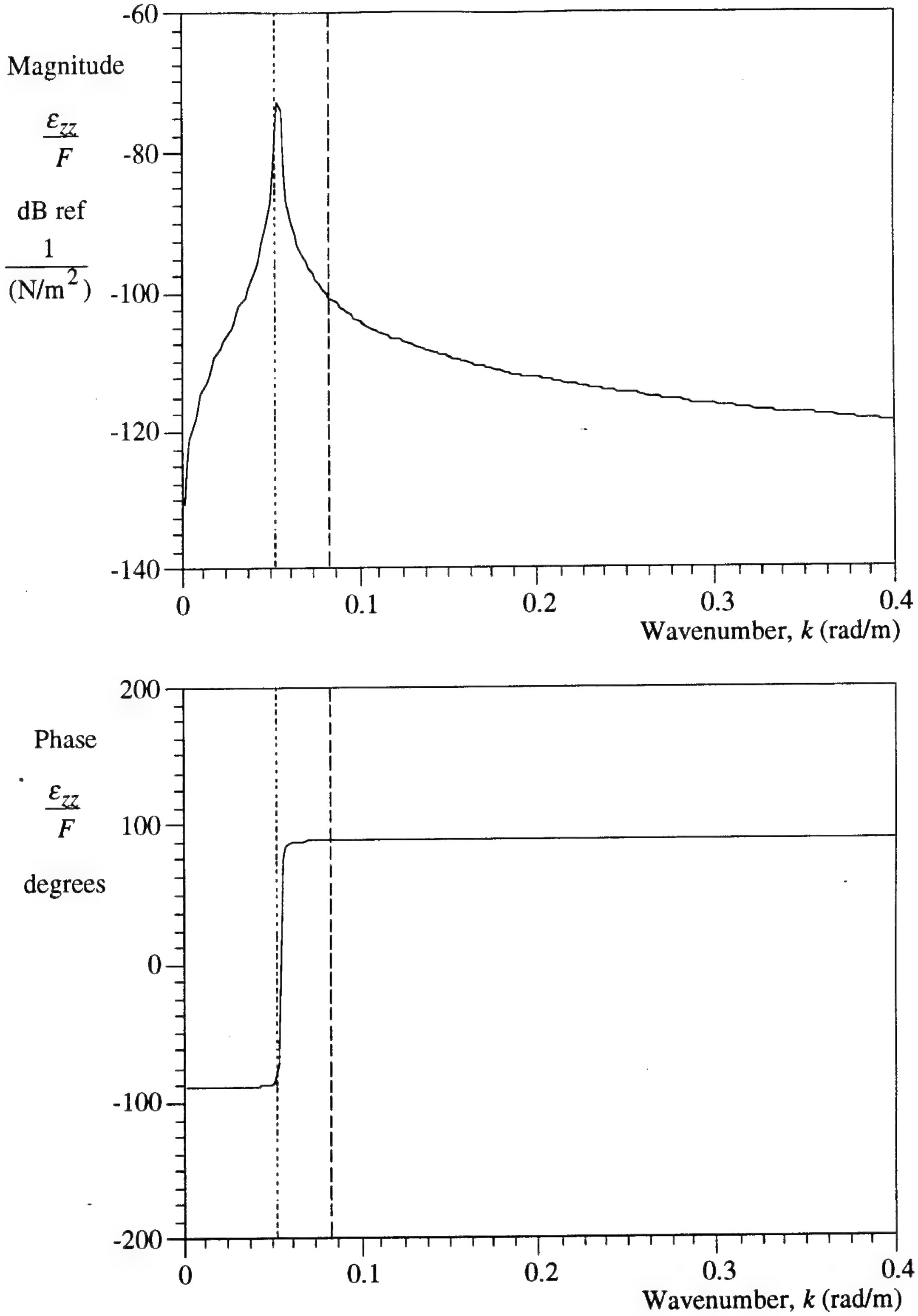

Figure 7. Transfer Function of Longitudinal Strain Divided by Shear Stress Versus Wavenumber for $f = 50$ Hz

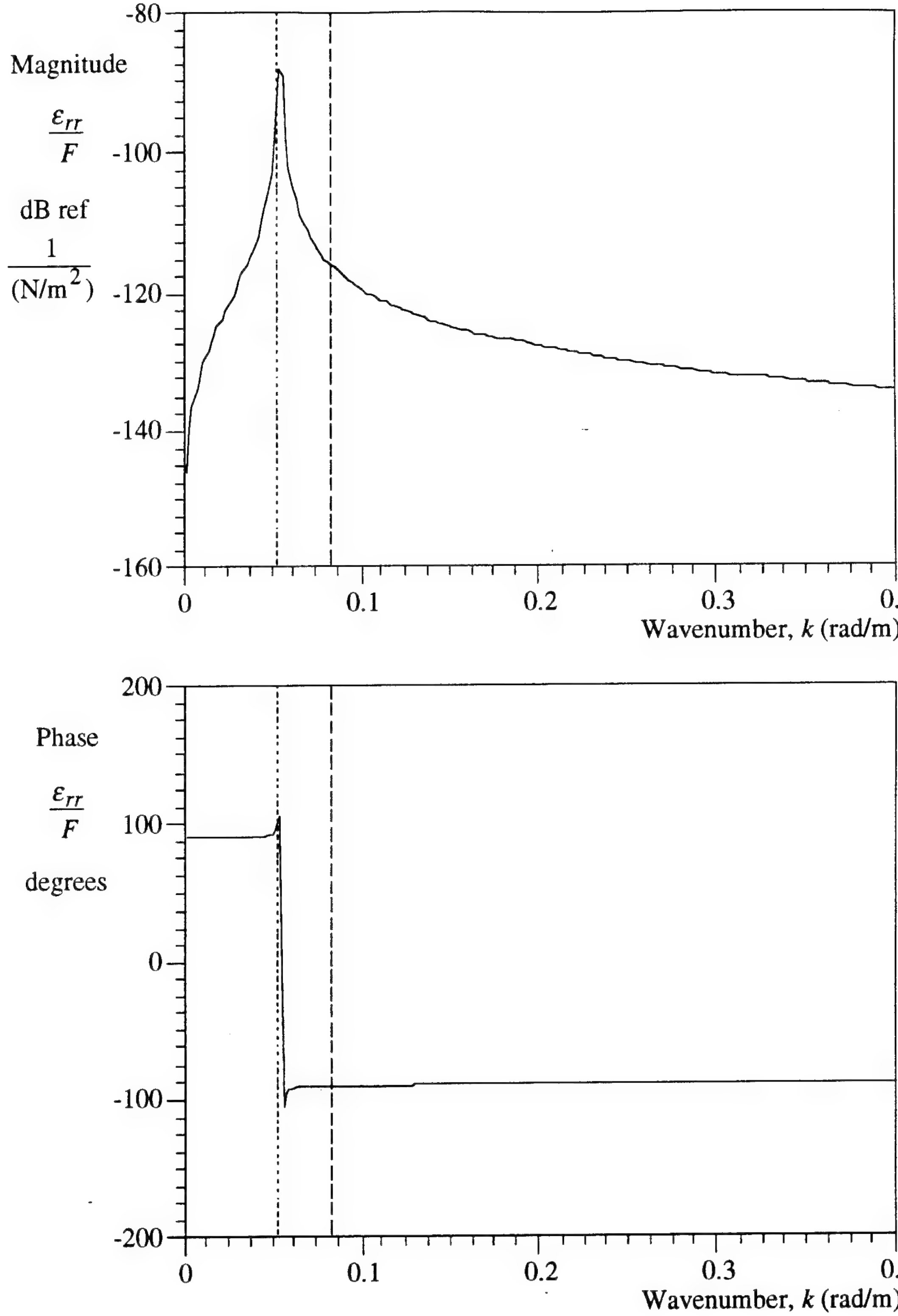

Figure 8. Transfer Function of Radial Strain Divided by Shear Stress Versus Wavenumber for $f = 50$ Hz

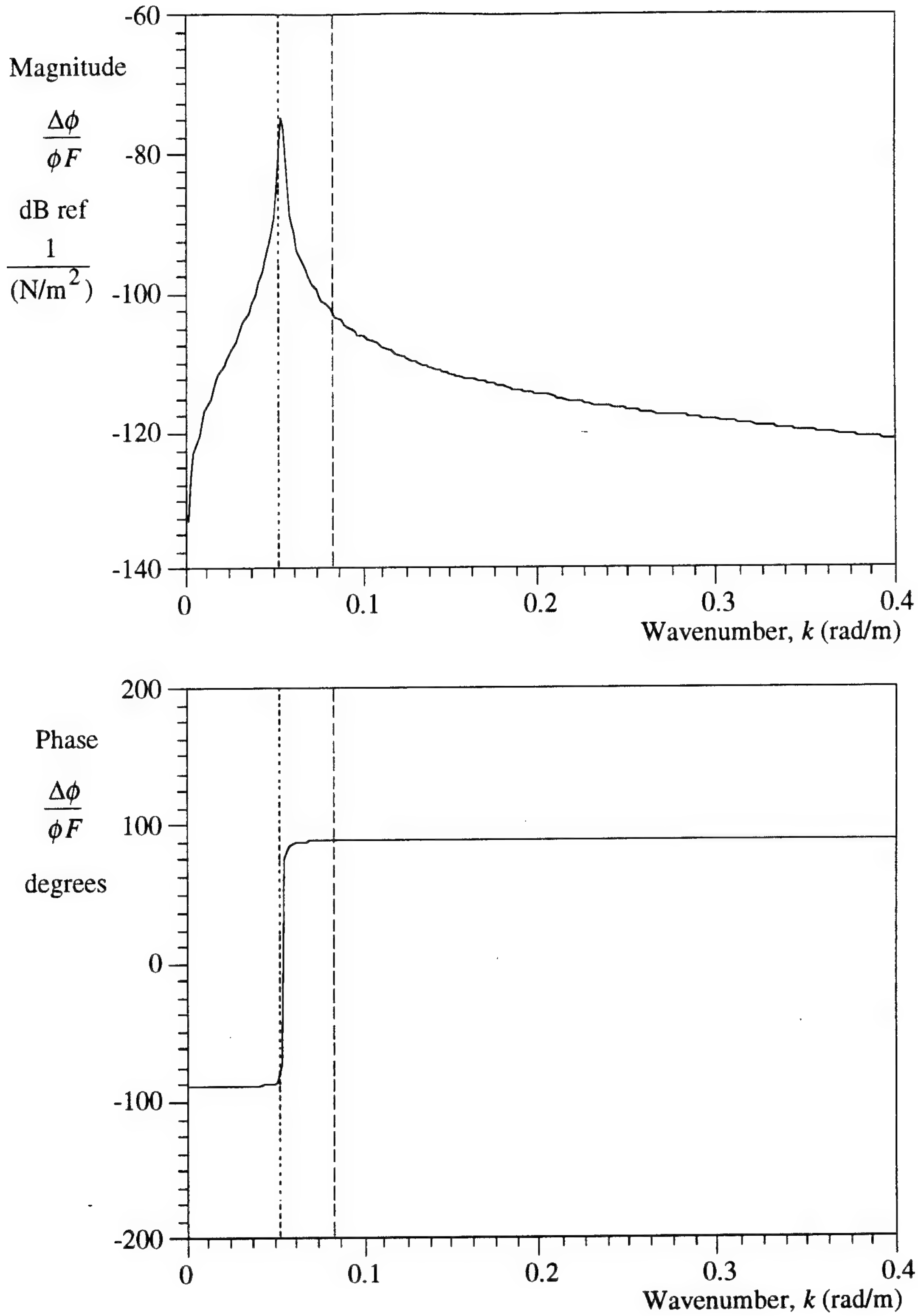

Figure 9. Transfer Function of Optical Phase Sensitivity Divided by Shear Stress Versus Wavenumber for $f = 50$ Hz

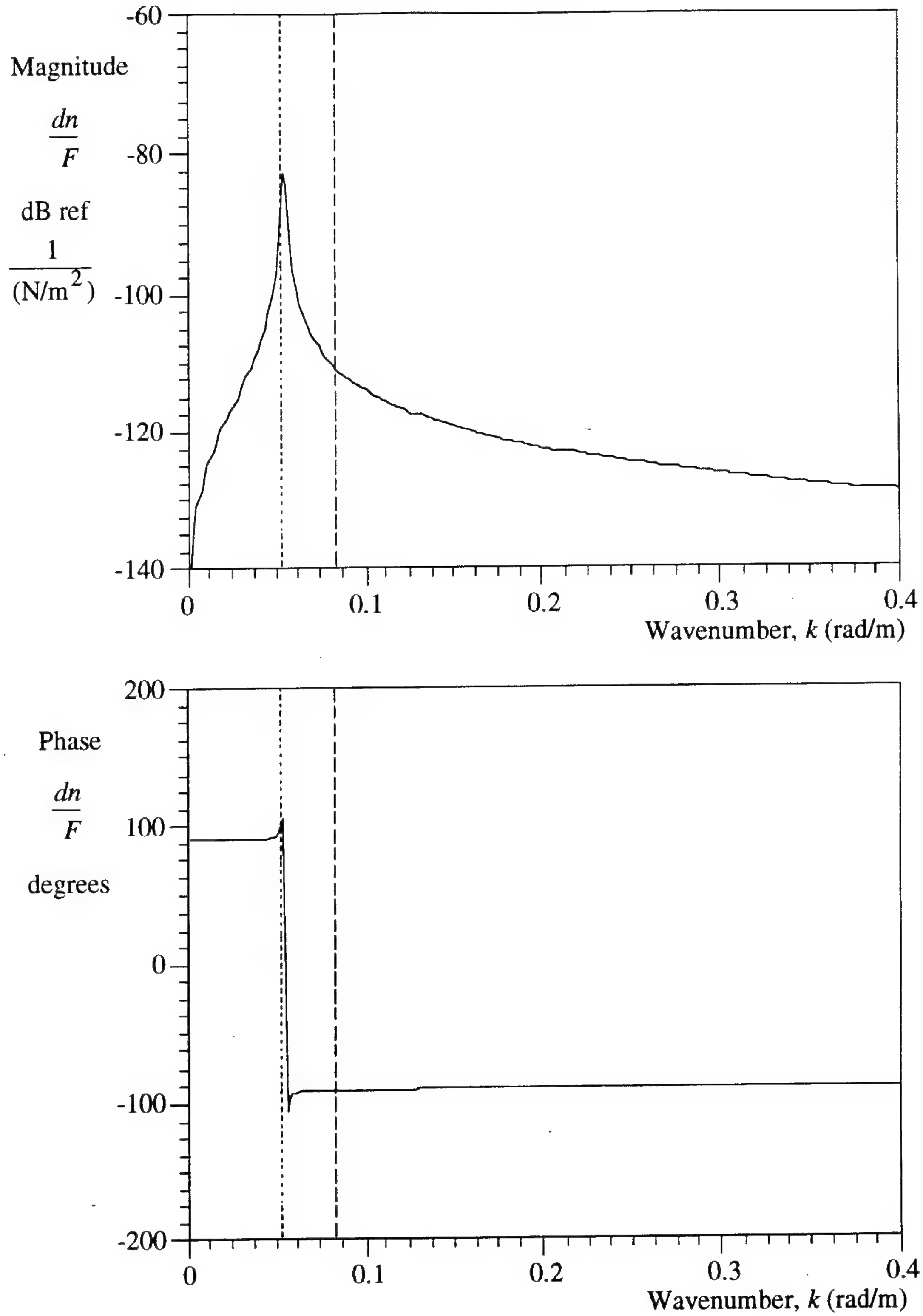

Figure 10. Transfer Function of Change of Refractive Index Divided by Shear Stress Versus Wavenumber for $f = 50$ Hz

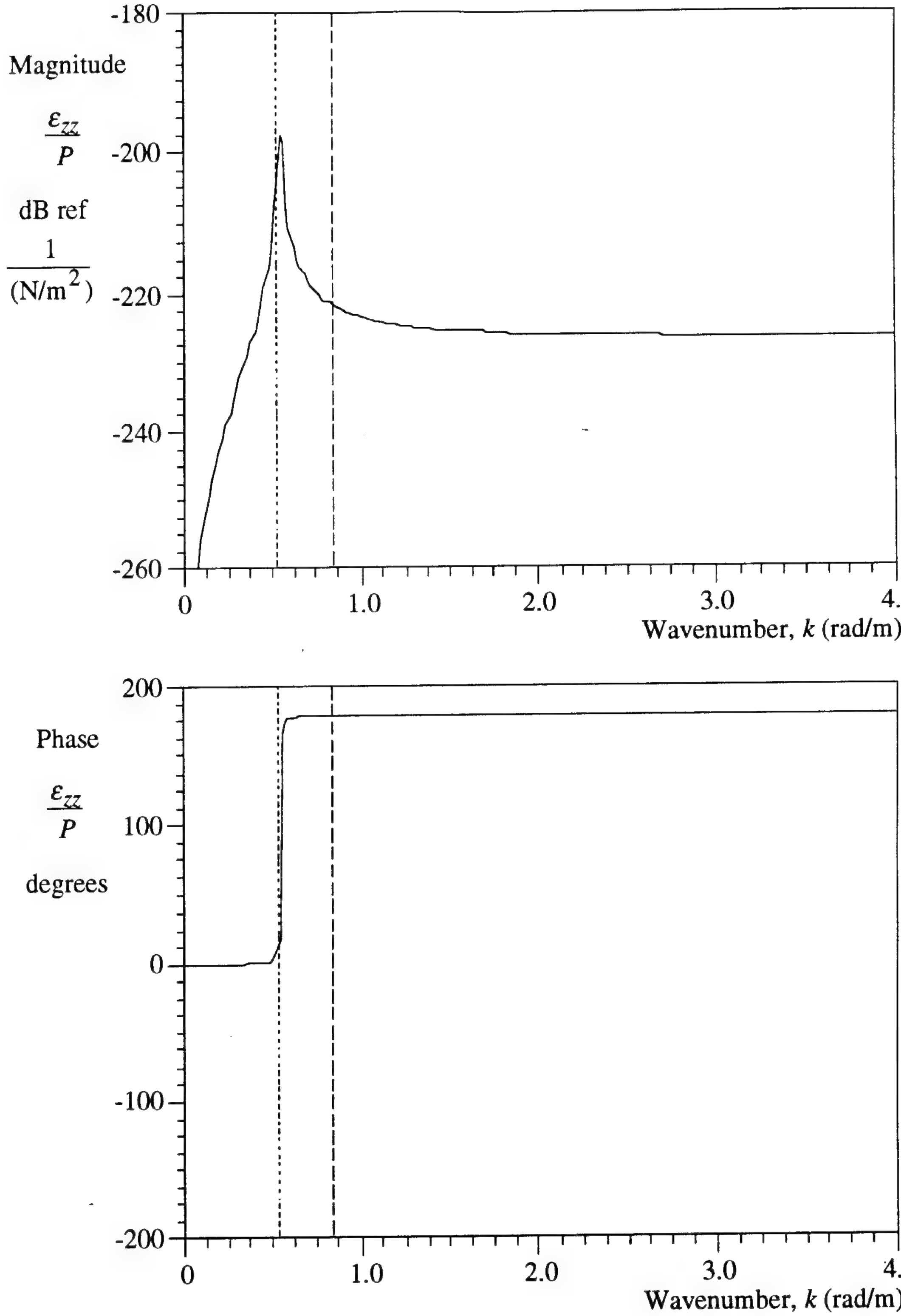

Figure 11. Transfer Function of Longitudinal Strain Divided by Normal Pressure Versus Wavenumber for $f = 500$ Hz

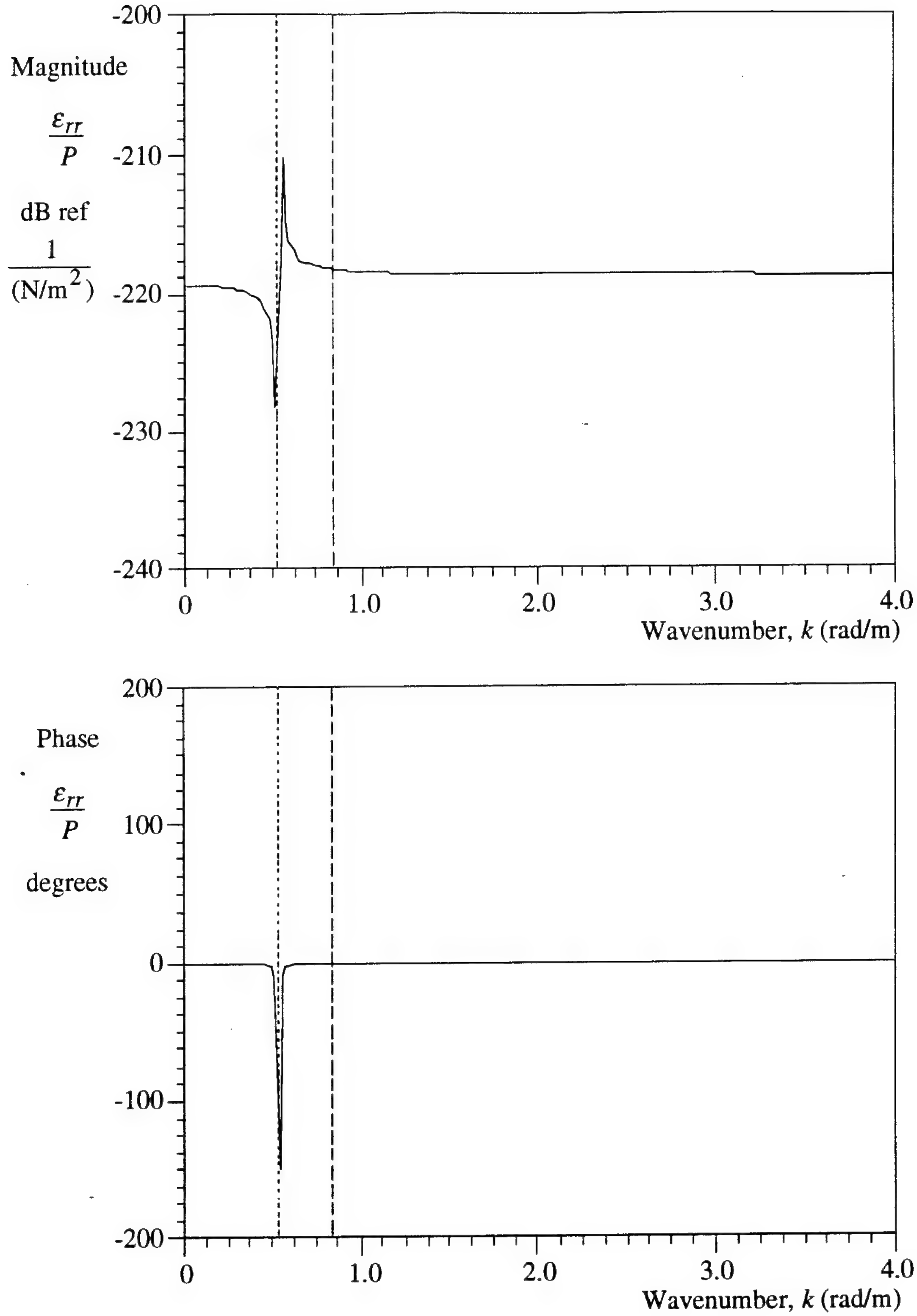

Figure 12. Transfer Function of Radial Strain Divided by Normal Pressure Versus Wavenumber for $f = 500$ Hz

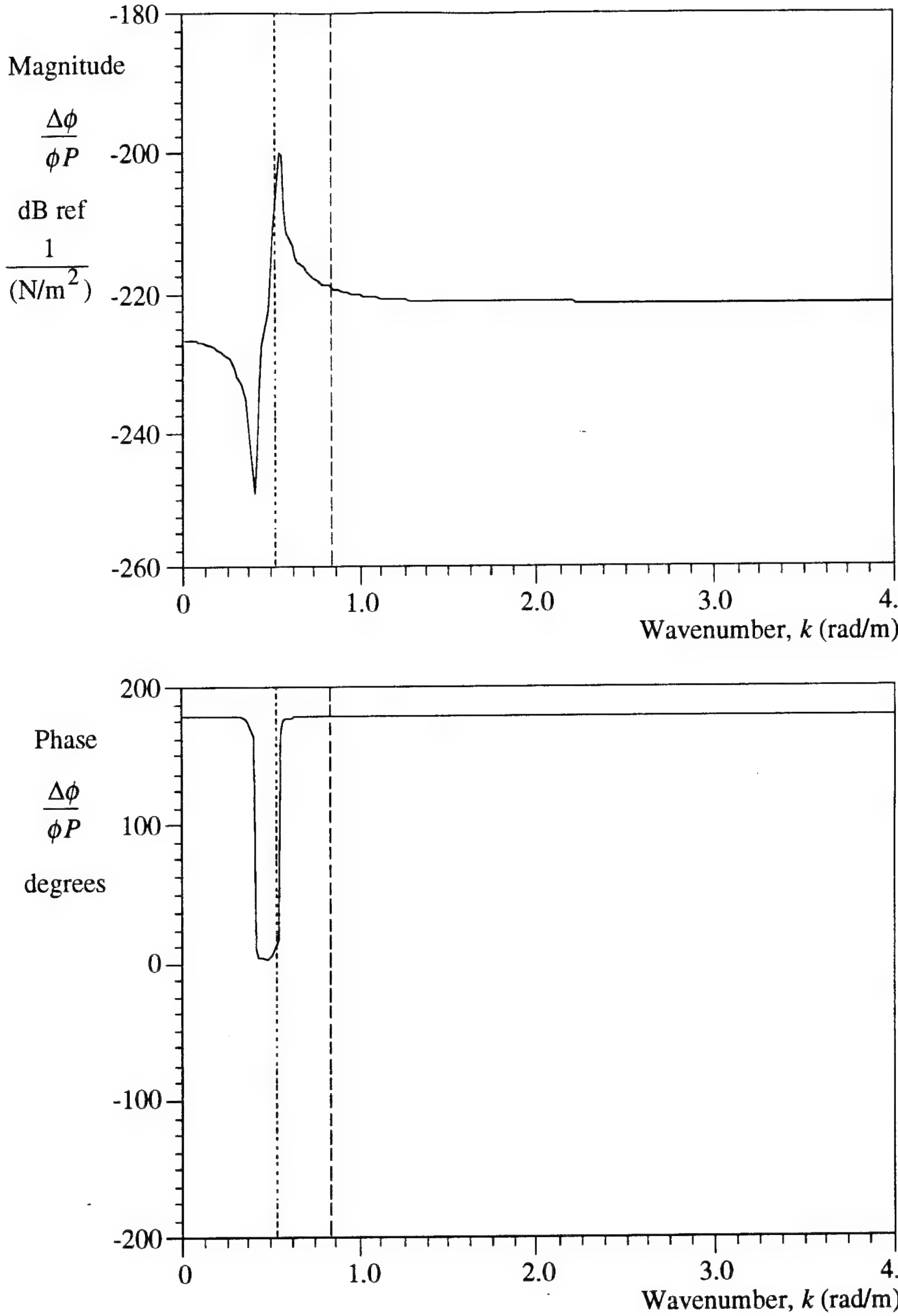

Figure 13. Transfer Function of Optical Phase Sensitivity Divided by Normal Pressure Versus Wavenumber for $f = 500$ Hz

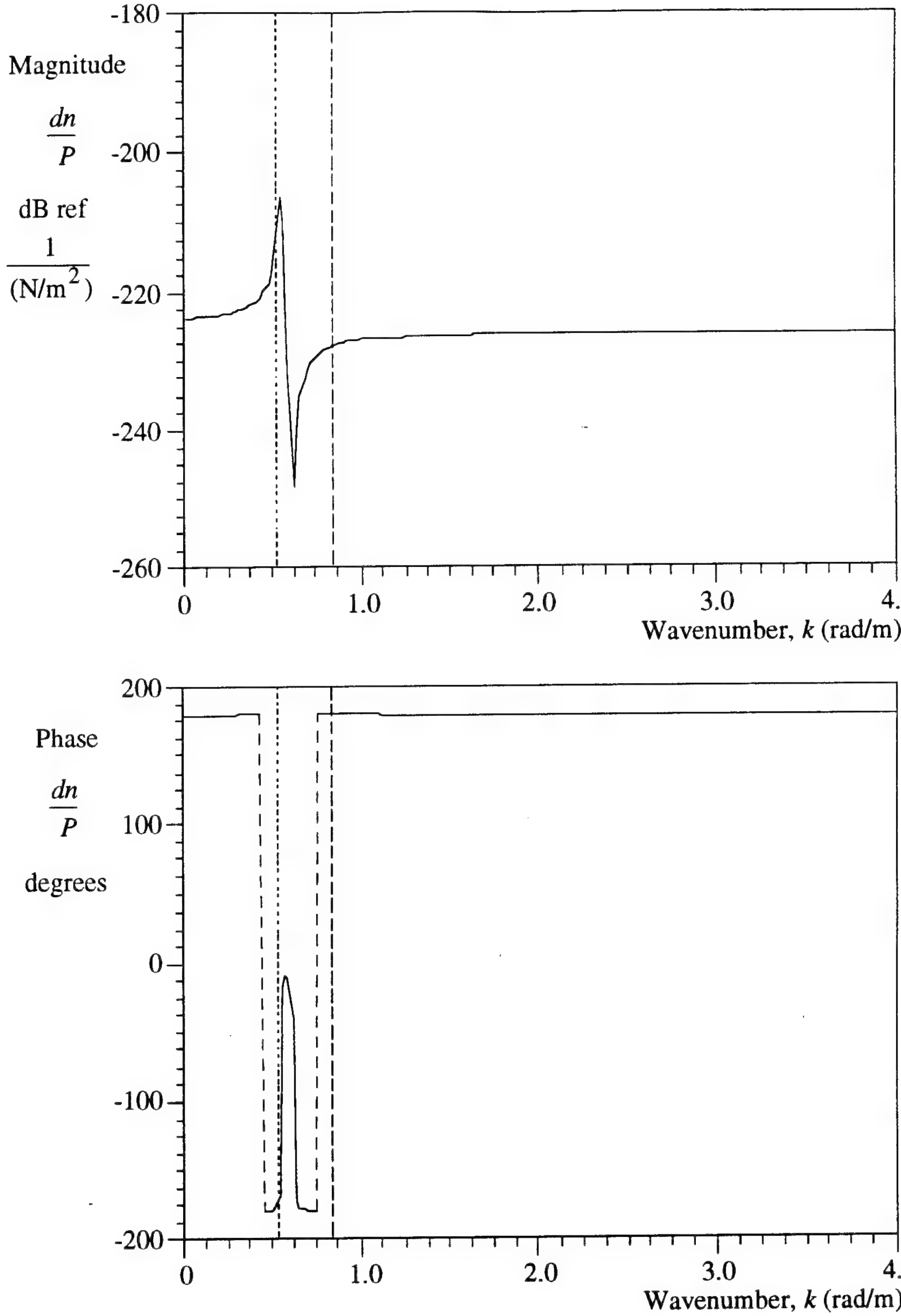

Figure 14. Transfer Function of Change of Refractive Index Divided by Normal Pressure Versus Wavenumber for $f = 500$ Hz

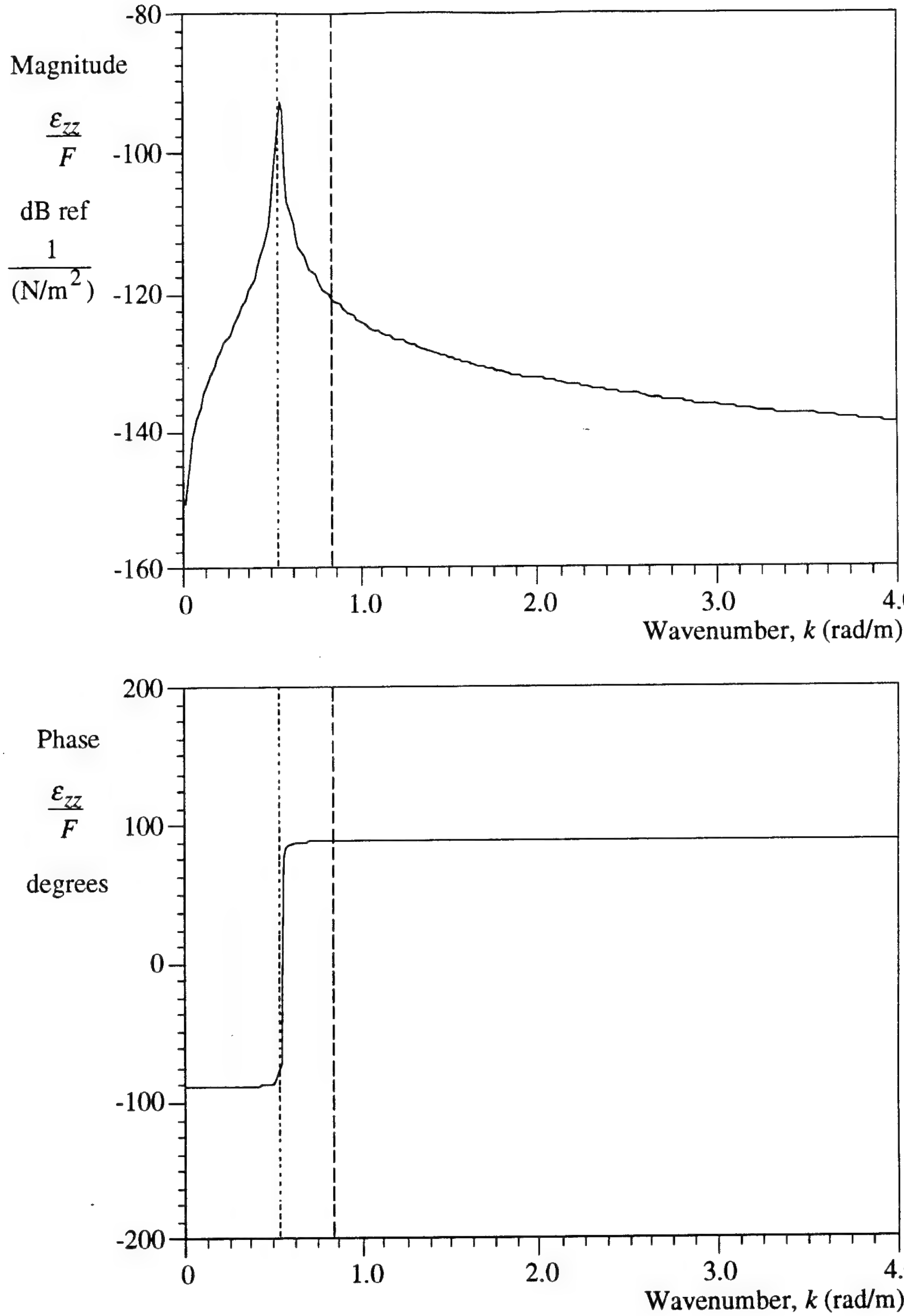

Figure 15. Transfer Function of Longitudinal Strain Divided by Shear Stress Versus Wavenumber for $f = 500$ Hz

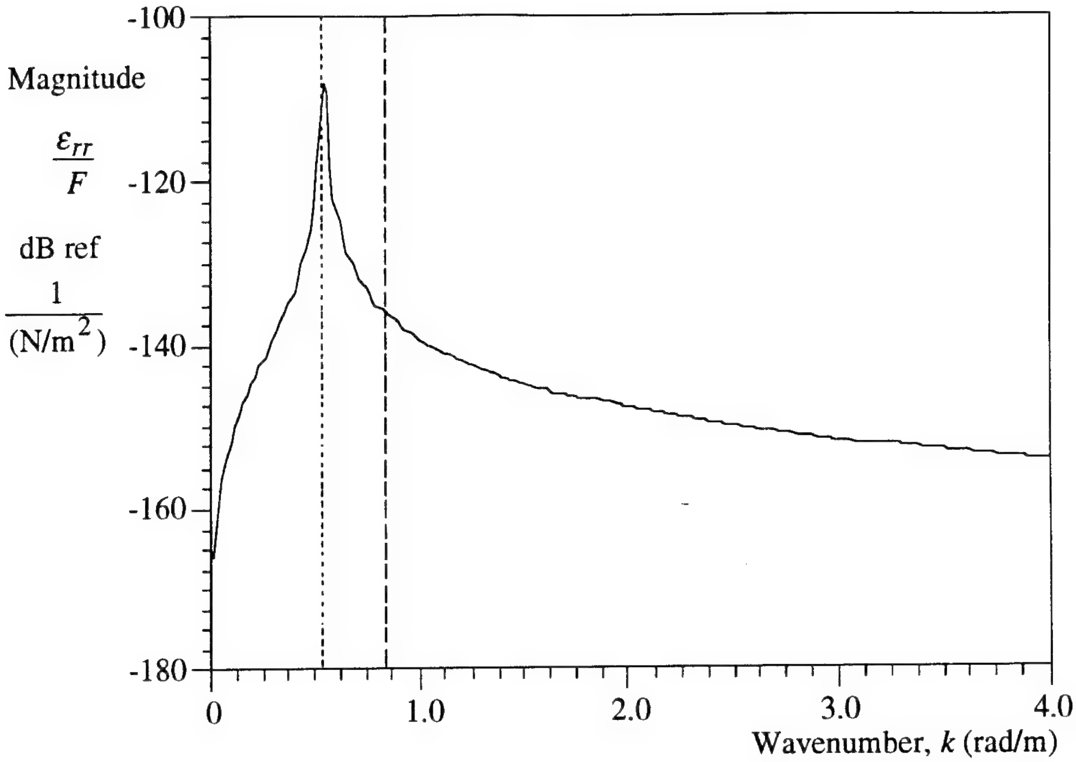

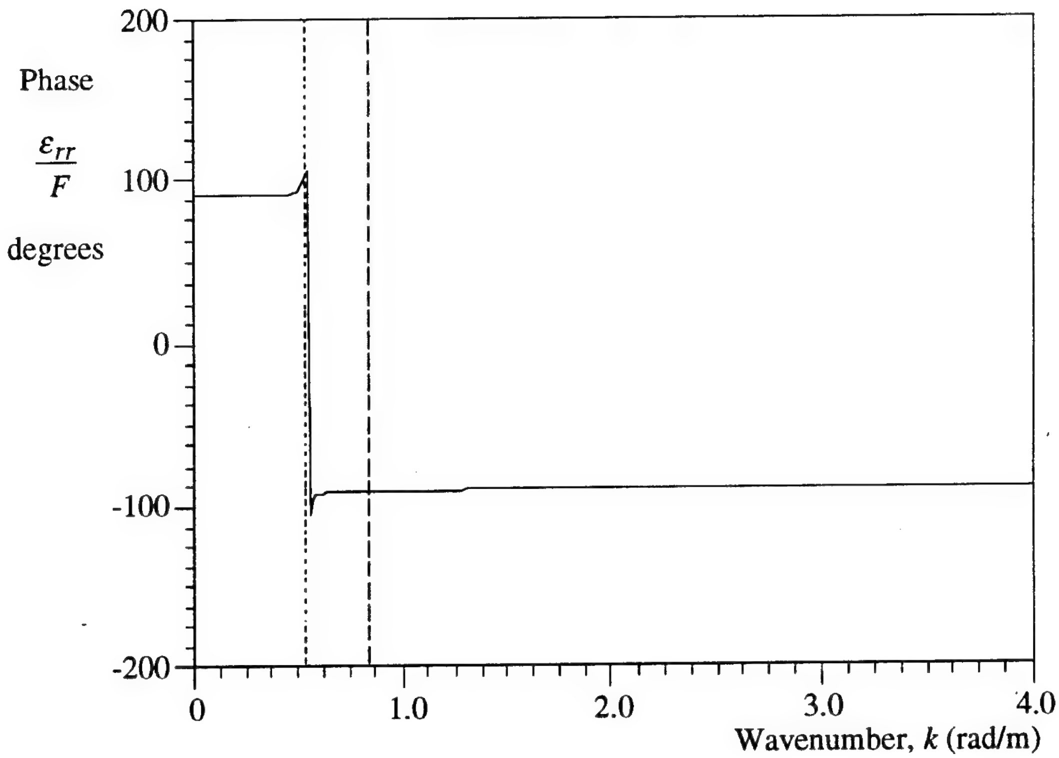

Figure 16. Transfer Function of Radial Strain Divided by Shear Stress Versus Wavenumber for $f = 500$ Hz

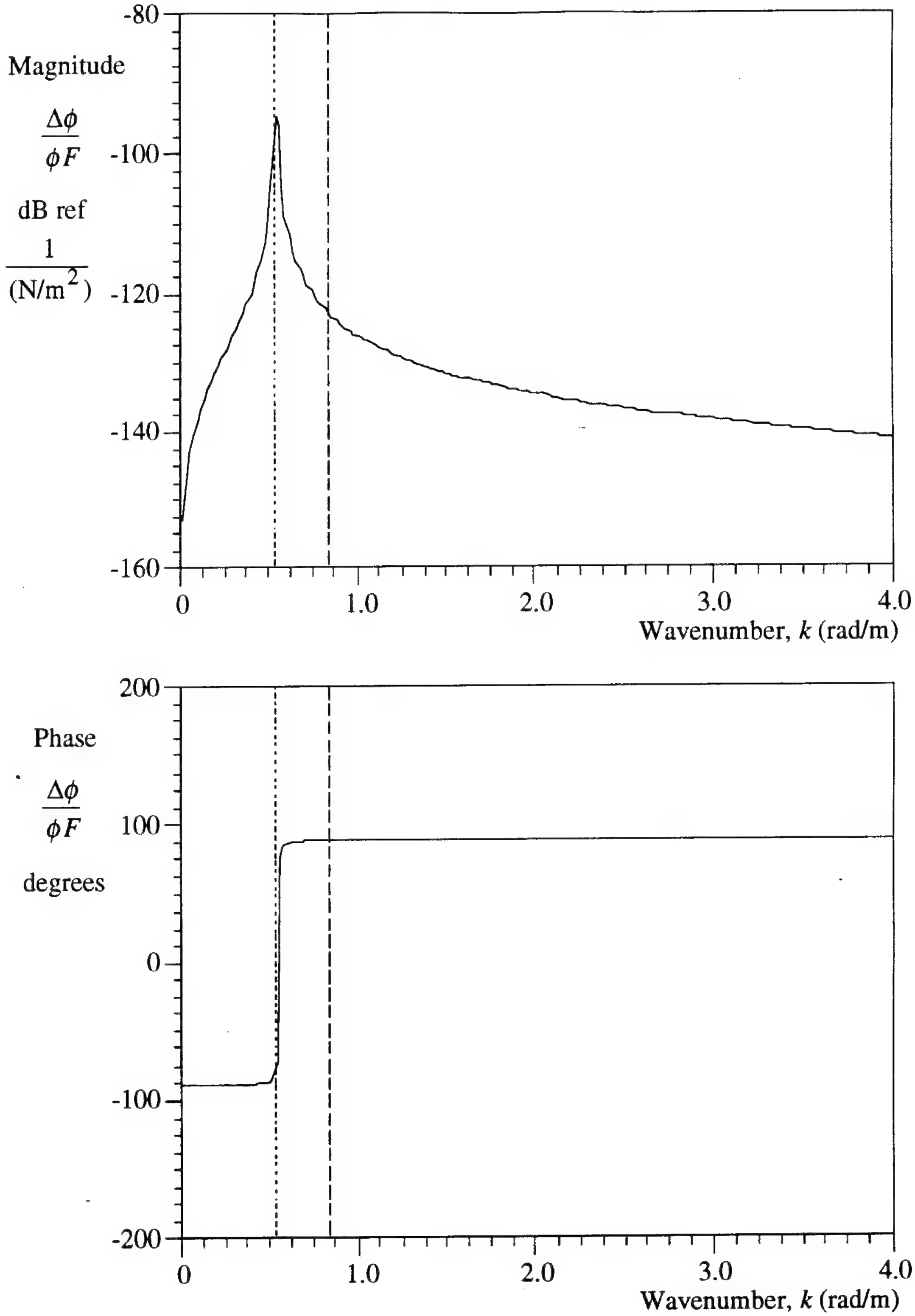

Figure 17. Transfer Function of Optical Phase Sensitivity Divided by Shear Stress Versus Wavenumber for f = 500 Hz

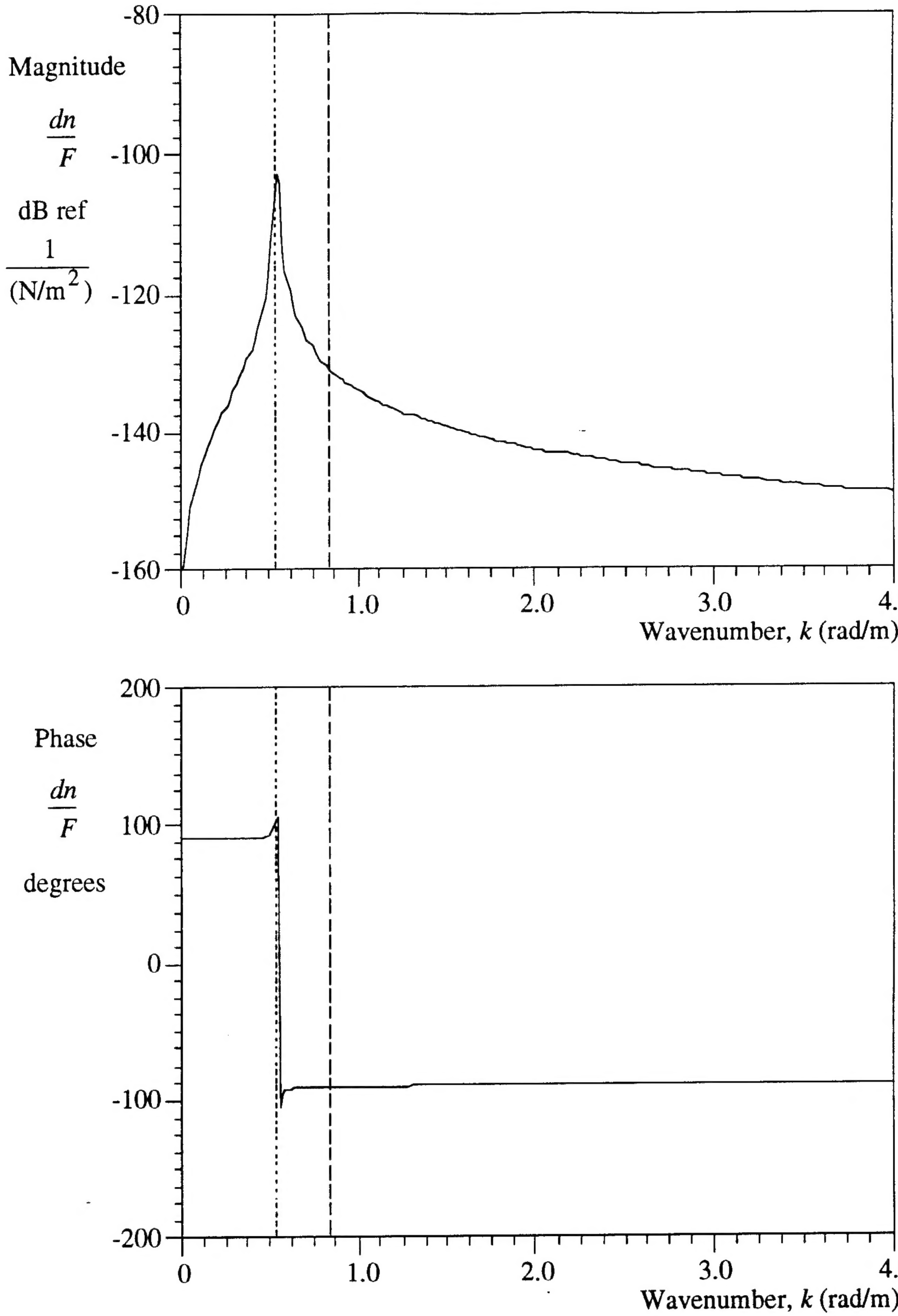

Figure 18. Transfer Function of Change of Refractive Index Divided by Shear Stress Versus Wavenumber for $f = 500$ Hz

6. REFERENCES

Cook, R. D., 1974, *Concepts and Applications of Finite Element Analysis*, John Wiley & Sons, New York.

Davis, C. M., Carome, E. F., Weik, M. H., Ezekiel, S., and Einzig, R. E., 1982, *Fiber Optic Sensor Technology Handbook*, Dynamic Systems, Inc., Reston, Virginia.

Graff, K. F., 1975, *Wave Motion in Elastic Solids*, Dover Publication, Inc., New York.

Holden, A. N., 1951, "Longitudinal Modes of Elastic Waves in Isotropic Cylinders and Slabs," *Bell Systems Technical Journal*, Vol. 30, pp. 956-969.

Kaul, R. K., and McCoy, J. J., 1964, "Propagation of Axisymmetric Waves in a Circular Semi-Infinite Elastic Rod," *Journal of the Acoustical Society of America*, Vol. 36, pp. 653-660.

Lagakos, N., and Bucaro, J. A., 1981, "Pressure Desensitization of Optical Fibers," *Applied Optics*, Vol. 20, No. 15, pp. 2716-2720.

Meeker, T. R., and Meitzler, A. H., 1964, "Guided Wave Propagation in Elongated Cylinders and Plates," *Physical Acoustics*, Vol. 1, Part A, Chapter 2, Academic Press, New York.

Potter, M. C., 1978, *Mathematical Methods in the Physical Sciences*, Prentice-Hall, Inc., Englewood Cliffs, New Jersey.

Timoshenko, S. P., and Goodier, J. N., 1934, *Theory of Elasticity*, McGraw-Hill Book Company, New York.

Zienkiewicz, O. C., 1983, *The Finite Element Method*, McGraw-Hill Book Company, New York.

APPENDIX - NUMERICAL EVALUATION OF THE BESSEL FUNCTION J

The complex Bessel function J was evaluated numerically. Based on the magnitude of the argument, this process used one of two equations. If the magnitude of the argument of z was less than 3.0, the equation

$$J_n(z) = \left(\frac{z}{2}\right)^n \sum_{k=0}^{16} \frac{(-z^2/4)^k}{k!\,(k+n)!} \tag{A-1}$$

was used. When the magnitude of the argument of z was greater than 3.0, an asymptotic expansion was used (where $|\arg z| < \pi$):

$$J_n(z) = \sqrt{\frac{2}{\pi z}}\left[A_n(z)\cos\left(z - \frac{n\pi}{2} - \frac{\pi}{4}\right) - B_n(z)\sin\left(z - \frac{n\pi}{2} - \frac{\pi}{4}\right)\right], \tag{A-2}$$

where

$$\begin{aligned} A_n(z) = 1 &- \frac{(4n^2-1)(4n^2-9)}{2!(8z)^2} + \frac{(4n^2-1)(4n^2-9)(4n^2-25)(4n^2-49)}{4!(8z)^4} \\ &- \frac{(4n^2-1)(4n^2-9)(4n^2-25)(4n^2-49)(4n^2-81)(4n^2-121)}{6!(8z)^6} \\ &+ \frac{(4n^2-1)(4n^2-9)(4n^2-25)(4n^2-49)(4n^2-81)(4n^2-121)(4n^2-169)(4n^2-225)}{8!(8z)^8} \end{aligned} \tag{A-3}$$

and

$$\begin{aligned} B_n(z) = &\frac{(4n^2-1)}{8z} - \frac{(4n^2-1)(4n^2-9)(4n^2-25)}{3!(8z)^3} \\ &+ \frac{(4n^2-1)(4n^2-9)(4n^2-25)(4n^2-49)(4n^2-81)}{5!(8z)^5} \\ &- \frac{(4n^2-1)(4n^2-9)(4n^2-25)(4n^2-49)(4n^2-81)(4n^2-121)(4n^2-169)}{7!(8z)^7} . \end{aligned} \tag{A-4}$$

INITIAL DISTRIBUTION LIST

Addressee	No. of Copies
Defense Technical Information Center	12
Naval Research Laboratory (T. Dandridge, N. Lagakos)	2
Naval Sea Systems Command (Capt. G. Kent (PMS-425), D. Lechner (PMS-42511))	2
Office of Naval Research 321 (T. Goldsberry, R. Varley, K. Dial, S. Littlefield, D. Davison)	5
Program Executive Office, USW/ASTO (Cdr. J. Polcari, W. Chen, A. Hommel, J. Jones, Lcdr. M. Traweek, R. Melusky)	6
Space And Naval Warfare Systems Command (J. Feuillet (PMW-182))	1